Hindawi
Advances in Materials Science and Engineering
Volume 2018, Article ID 1952671, 16 pages
https://doi.org/10.1155/2018/1952671

Research Article

Experimental and FEM Research on Airport Cement Concrete Direct-Thickening Double-Deck Pavement Slabs under Aircraft Single-Wheel Dynamic Loads

Qingkun Yu,[1] **Liangcai Cai**,[1] **and Jianwu Wang**[2]

[1]*Air Force Engineering University, Xi'an, Shaanxi Province, 710038, China*
[2]*Air Force Service Academy, Xuzhou, Jiangsu Province, 221000, China*

Correspondence should be addressed to Qingkun Yu; 1028419220@qq.com

Received 15 April 2018; Revised 11 July 2018; Accepted 22 July 2018; Published 10 October 2018

Academic Editor: Antonio Boccaccio

The wide-use airport cement concrete direct-thickening double-deck pavement slabs (ACCDDPS) were selected as the research object to study their mechanical properties. The airport runway simulation test station (ARSTS) was used to conduct indoor tests to demonstrate the distribution of tension stress at the bottom of slabs and slabs deflection. Furthermore, ANSYS software was applied to establish finite element model (FEM) of ACCDDPS and analyze the mechanical laws under different loads. The indoor tests results are in good agreement with the ANSYS simulation results, and some consistent conclusions can be obtained that the maximum tension stress increases with wheel load, and the slab middle of the longitudinal edge is a critical position. In addition, we studied the influence of covered layer thickness, elastic modulus, and slab size on pavement slab mechanical properties by ANSYS, and we concluded that although the structural parameters are different, the critical position of ACCDDPS is still in the middle of the longitudinal edge. However, for the covered layer and the original surface layer, the law that the tension stress values vary with the structural parameters is different, but the maximum deflection value is about 0.1.

1. Introduction

The cement concrete pavement has the advantages of large rigidity, strong bearing capacity, and good weather resistance and becomes the main form of airport pavement in many countries in the world. In the twenty-first century, there is a new question whether the pavement can meet the new aircrafts' application requirements, because many airport runways were constructed in the mid-to-late twentieth century, and most airport pavements have suffered different degrees of damage. Taking economic conditions, environmental benefits, and usage requirements into overall consideration, many countries have reinforced the existing old cement concrete pavement, which is commonly known as pavement coverings.

At present, pavement coverings can be made of asphalt and cement concrete. However, due to the asphalt pavements' short service life and poor corrosiveness to fuel oil, the cement concrete pavement, which has the advantages of good economy, high carrying capacity, and good durability, is the preferred choice for many airports. In addition, there are three kinds of structural forms for the pavement coverings, which are isolated covered layer, combined covered layer, and direct covered layer [1]. The direct covered layer is widely used because of its simple construction, low cost, and high performance. However, the traditional design theories and methods for thickening and reinforcing cement concrete pavement are out of date. Therefore, there is an urgent need to study the performance of ACCDDPS under the action of various types of aircrafts in order to develop new design theory.

The ACCDDPS mentioned in this paper means that the cement concrete thickened layer is directly laid on the clean old concrete cement pavement surface, which is characterized of a certain adhesive force and frictional resistance between the upper and lower two layers, resulting in a better overall stiffness in the upper and lower slabs. As shown in Figure 1, from the bottom to the top, the ACCDDPS

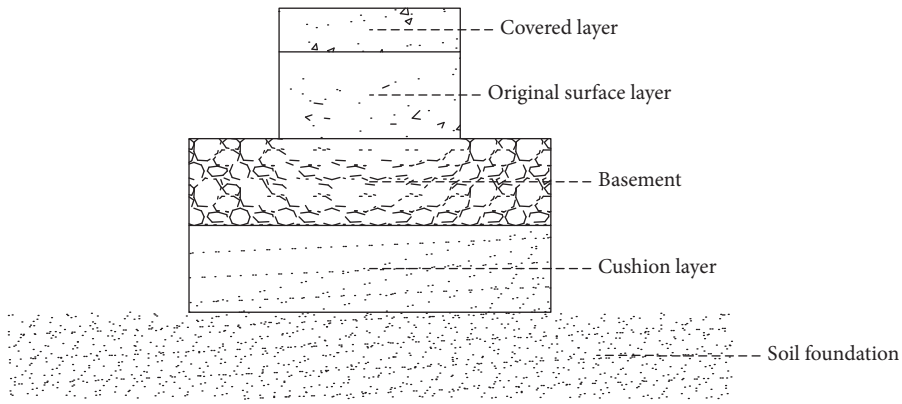

Figure 1: The ACCDDPS structure.

structure is composed of the natural soil foundation, the cushion (as appropriate), the compacted basement, the original surface layer, and the covered layer. When the covered layer is under construction, it is necessary to repair some functional damage that occurred in the original surface layer and to clean the entire pavement surface.

Since the first cement concrete double-deck slabs was built in the United States in 1930, the cement concrete double-deck slabs has been widely applied to the highway and airport in many countries, and the related research and practical exploration have also been carried out in full swing.

An improved solution algorithm based on Finite Element Method for dynamic analysis of rigid pavements under moving loads [2] is presented to research on the effect of soil modulus, shear modulus, pavement thickness, and the vehicle–pavement interaction.

Binchen et al. [3] established a fine airport pavement finite element model based on the Winkler foundation model to analyze the number of slabs required when the wheel loads are applied to the slab center, slab edges, and slab corners. Through analysis, he gave some suggestions: when the load is at the middle of the slab, it is recommended to establish a four-slab model; when the load is at the slab edge, two- or four-slab models are established; when the load is at the slab corner, it is recommended to establish four-slab model.

Shuyuan [4] analyzed, respectively, the load stress of isolated covered and direct covered cement concrete pavement slabs based on elastic half-space foundation and gave the moment calculation formulas of isolated covered cement concrete pavement slabs and the maximum tension stress of direct covered cement concrete pavement slab.

Chao et al. [5] applied ABAQUS software to analyze the influence of different materials at the original base (i.e., different strength) on the stress of pouring cement concrete surface after the old pavement is crushed. The analysis showed that some materials (such as the cement stabilized grit, the graded gravel, and the lime-ash soil) as the original base layer, the tension stress of the surface layer slab gradually decreases with the increase of the elastic modulus of the base material.

Haiyan et al. [6] used the theory of multilayer thin plates based on the elastic foundation model to explore the deflection and maximum stress of the double-deck pavement slab. On the basis of certain assumptions, the design methods of direct and isolated pavement structures are obtained by numerical calculation. Comparing with the analysis result of ANSYS software, it is found that the numerical calculation results can be well matched with the results of ANSYS analysis, which proves the feasibility of the method to some extent.

Xiangcheng et al. [7] firstly established a 3D finite element model to analyze the effect of fiber gratings on the maximum tension stress at the bottom of the covered layer slab. Due to the addition of the fiber grid, the friction coefficient between the covered layer and the original surface layer is changed that the tension stress gradually decreases as the friction coefficient increases, and the tension stress tends to be stable until the friction coefficient is 0.8. In addition, he adopted orthogonal test to analyze the influence of the thickness and elastic modulus of covered layer, the size and elastic modulus of the fiber grid, the elastic modulus of the original covered layer and compacted soil layer on the maximum principle stress and the defection at the bottom of the covered slab, and the tension stress at the bottom of the original surface layer.

Xianmin et al. [8] established 3D finite element models for airport runways, selected 5 types of aircrafts (A320-200, B737-800, A340-500, B777-200, and B747-300, resp., divided into 2 groups in terms of the same load level and different landing gear configuration) to analyze the influence of different landing gear configurations (including the number of wheels, landing gear spacing and landing gear layout, and other factors) on the pavement surface deflection, impact depth on the base depth, and the maximum tension stress at the bottom of surface layer. The analysis results show that with the same load, the fewer the number of wheels, the greater the deflection of the slab bottom, the greater the maximum tension stress; the greater the landing gear spacing, the smaller the impact depth on the base.

Zizheng and Hongduo [9] analyzed the structural response of the double-deck cement concrete pavement slab under the action of a large-scale aircraft with relatively complicated landing gear configuration represented by A380-800 through ABSQUS software, combined with the pavement fatigue life under different load distributions

according to the space superposition effect and finally obtained the most unfavorable load combination of A380-800.

Xiang [10] established a 3-D finite element model of a composite airport pavement with nine panels and chose B777-200 aircraft as the calculation load. The bottom tension stress of the cement concrete slab is selected as the index to analyze the most unfavorable position of the composite airport pavement; the orthogonal test design is applied in studying the influence of pavement structural parameters on load stress.

The above research achievements mainly use finite element method to simulate the airport pavement slab, which inspire us to conduct ACCDDPS research by FEM. The predecessors have established the FEM under the role of the B777-200 and A380-800 models and studied the different effects of the pavement structure parameters. However, no relevant work has been carried out on ACCDDPS under the action of various main aircrafts, which is necessary to conduct this research because many airports' cement concrete pavements undertake the task of guaranteeing various types of aircrafts. Moreover, the experimental method and FEM method have not been compared in order to draw more scientific conclusions.

Taking four main aircrafts of A, B, C, and D as an example, we design the ARSTS experiment on ACCDDPS under different loads. The stress distribution and slab deflection are analyzed by the cyclic-load mechanical test on the ACCDDPS. On the basis of fully simulating the experimental conditions, we intend to establish an ACCDDPS FEM by ANSYS software. The FEM results and experimental results will be compared and analyzed, which should be compared with the existing research results to verify the credibility and accuracy of our research. Moreover, we will consider and analyze the influence of covered layer thickness, elastic modulus, and slab size on pavement mechanical properties by FEM, in order to draw some fruitful conclusions to guide the design, construction, and maintenance of the ACCDDPS.

2. Airport Runway Simulation Test Station Experimental Research on ACCDDPS under Aircraft Single-Wheel Dynamic Loads

2.1. Experimental Equipment, Materials, and Methods

2.1.1. Simplified Design of Experiment. The size of an ACCPPDS is generally more than 5 m × 5 m. Due to the limitations of the ARSTS experimental equipment, indoor experiments cannot be performed in a ratio of 1 : 1. Based on similarity theorems, the simplified designs are as follows:

(1) Ignore the influence of natural environment and other factors on the experimental conditions, including groundwater level change, temperature change and humidity change.

(2) The plane size and thickness of each pavement slab are reduced to a certain proportion according to the geometric similarity. The size of the test slab is 0.50 m × 0.50 m × 0.25 m, ignoring the lateral restraining effect.

(3) Ensure that the construction process in specimen's production part is the same as in practice, ignoring the influence of human factors during the whole process of the experiment.

(4) Suppose that the old and new surface layer, basement, and soil foundation are continuous, homogeneous, and isotropic perfectly linear elastic bodies.

2.1.2. Airport Runway Simulation Test Station. ARSTS was designed by a Changchun Experimental Instrument Company in September 2012, called Model KPD-01. This instrument simulates the movement of a wheel on a runway by regulating the size of wheel load and replacing wheels with different sizes. In addition, through the introduction of stress-strain collectors, the relevant data of pavement surface and basement can be collected, further analyzing the force conditions of the pavement.

ARSTS is mainly composed of three parts: the main part, the power system, and the human-computer interaction system, as shown in Figure 2.

2.1.3. Raw Materials and Mix Proportions. The main materials of specimens are ordinary Portland cement, medium sand, gravel, and water whose performance conforms to the provisions [1].

According to the requirements for ordinary cement concrete mix proportions [11], combined with relevant specifications on ACCDDPS, the mix proportions are shown in Table 1.

2.1.4. Equipment Preparation. The basement and soil foundation in the ARSTS box are treated as follows: fill the clay, and compact it layer by layer until it reaches a thickness of 0.70 m. Then, pave the gravel and tamp it layer by layer until the thickness is about 0.3 m, as shown in Figure 3.

In this experiment, stress gauges are placed at the bottom of the ACCDDPS specimen. Due to the symmetry of a square specimen, we only need to collect the stress values of 1/4 specimen. The layout of the measuring points is shown in Figure 4.

2.1.5. Specimens Production and Curing. The concrete steps of ACCDDPS specimens are shown below:

(1) Mold: make double-deck slab mold, size: 0.50 m × 0.50 m × 0.25 m, wood material. Considering the later stripping problem, a layer of plastic film is laid in the mold, and then a small amount of lubricating oil is brushed in the plastic film.

(2) Pouring concrete: firstly, an already accomplished single-layer cement concrete slab (0.50 m × 0.50 m × 0.25 m) is placed in the mold, and the stress gauges are pasted at 9 positions as shown in Figure 4. Secondly, make the thickening layer, uniformly pour cement concrete on the single-layer slab, tamp with a vibrator, flatten to a design thickness, and level the surface.

Figure 2: The ARSTS.

Table 1: Cement concrete material consumption per cubic meter.

Concrete materials	Cement	Water	Sand	Gravel	
				Large grain- size	Small grain-size
Weight (kg)	315	145	637	859	531

Figure 3: The ARSTS box preparation.

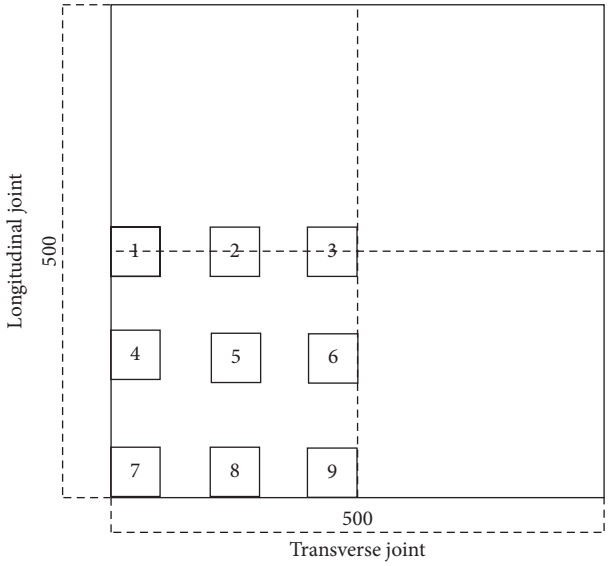

Figure 4: The stress gauges layout schematic diagram.

(3) Conservation: the wet geotextiles are covered on the specimens for curing. During the period, spray an appropriate amount of water daily to ensure the required moisture during the curing period.

(4) In the same steps (1) to (3), three tests are required under each aircraft load, so 12 specimens are to be poured.

The process of making ACCDDPS specimens is shown in Figure 5.

2.1.6. Experiment Procedures

(i) ARSTS Debug. Fix the cured specimens in ARSTS box, connect, and check the line. Open the experiment software system. Set the load in the vertical direction to 10 kN and slowly lower the wheel to the specimen. Observe whether the data display on the software system; if yes, continue subsequent operations; if not, recheck lines and trouble shoot problems until the data display normally.

(ii) Set Experimental Relevant Parameters. The experiment parameters are set as shown in Table 2.

(iii) Data Collection. Collect the value of the surface deflection, the maximum tension stress at the bottom of the slab, and the number of repeated action when the specimen is fractured. Considering that the maximum number of annual flight times for the four main aircrafts of A, B, C, and D is 25000, the number of repeated action is controlled to 30000 times in order to ensure the successful progress of the experiment.

(iv) Adjust the Load and Start the Experiment. The aircraft single-wheel dynamic loads are applied to the ACCDDPS

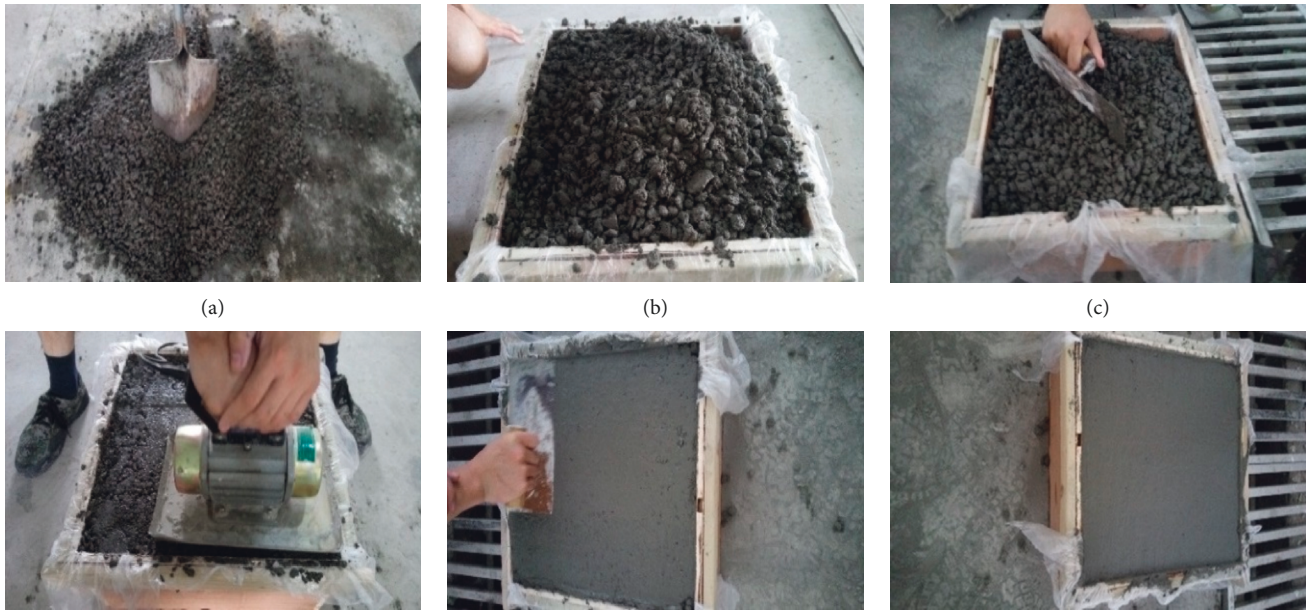

Figure 5: The making process of specimens. (a) Mixing. (b) Filling. (c) Leveling. (d) Tamping and mud extracting. (e) Rendering. (f) Finishing.

Table 2: Experiment relevant parameters.

Loading mode	Parameters						
	Control mode	Frequency (Hz)	Max/min Load (kN)	Max/min displacement (m)	Load wave	Recycle times	Protection Load (kN)
Vertical load	Displacement	1 Hz	86.64/0	Default	Sine	3000	200
Horizontal load	Displacement	1 Hz	Default	0.23 m/−0.23 m	Sine	3000	Default

specimens through the ARSTS wheel simulator, referring to partial parameters of A, B, C, and D four main aircrafts in Table 3.

Set the vertical load to 86.64 kN, and start the experiment. In the course of the experiment, pay close attention to the wheel running to ensure that the wheel does not deviate from the specimen. When the specimen is completely broken, the experiment is stopped immediately, and the relevant data are recorded. Continuing with other experiments, the vertical loads of the wheel are sequentially set to 103.07 kN, 129.16 kN, and 196.52 kN, and the other procedures are the same as above.

2.2. ARSTS Experiment Results. In order to reduce the experimental error, we choose the average value of three sets of experimental results at the same load level as the final value, and the detailed method of taking value refers to a Chinese professional standard "Specifications for Airport Cement Concrete Pavement Design"(MH/T5004-2010). The tension stress values are shown in Table 4, and the total surface deflection values are shown in Table 5.

In order to express the experimental results more directly and vividly, draw Figures 5–8 according to the above data.

As depicted in Figures 6 and 7, for both covered layer and original surface layer, the maximum tension stress is at the measuring point 1, followed by the measuring point 9, and the minimum tension stress is at the measuring point 5, which shows that the critical position of ACCDDPS is in the middle of the longitudinal edge.

As shown in Figure 8, the tension stress of covered layer increases with the increase of wheel load. When the load increases from 129.16 kN to 196.52 kN, the maximum tension stress increases to 0.26 MPa. That is, at the point of 129.16 kN, there is a clear inflection point, and after that point, the change rate of stress with load becomes larger. Similarly, the tension stress of original surface layer also increases with the increase of wheel load; however, the rate of growth has been slightly increased after the point of 129.16 kN.

Figure 9 shows that the total deflection of surface layer increases with the increase of wheel load, and the rising rate is relatively stable with no large fluctuations.

3. ACCDDPS FEM Establishment by ANSYS Software

3.1. Basic Assumptions. Before modeling the ACCDDPS, considering the differences between the ANSYS FEM and

Table 3: Four main Aircrafts' partial parameters.

Aircraft	Single main wheel grounding area (cm^2)	Single main wheel dynamic load (kN)	Single main wheel static load (kN)	Maximum takeoff masskg)	Landing gear Configuration	Main wheel tire pressure (MPa)
A	1110.77	86.64	72.20	6200	Double-axis double-wheel	0.78
B	1171.25	103.07	85.89	75800	Double-axis double-wheel	0.88
C	2483.85	129.16	107.63	191000	Compound	0.52
D	1284.44	196.52	157.22	34500	Single-wheel	1.53

Table 4: The tension stress at the slab bottom.

Gauge position	Tension stress stress (MPa)	Wheel Load (kN)			
		86.64	103.07	129.16	196.52
Covered layer bottom	1	0.1269	0.1445	0.1754	0.2601
	2	0.0832	0.1143	0.1305	0.1951
	3	0.0741	0.0995	0.1241	0.1701
	4	0.1157	0.1321	0.1543	0.2245
	5	0.0945	0.1209	0.1462	0.2069
	6	0.0842	0.1024	0.1322	0.1902
	7	0.1221	0.1401	0.1609	0.2379
	8	0.1146	0.1311	0.1507	0.2157
	9	0.1234	0.1421	0.1721	0.2542
	max	0.1269	0.1445	0.1754	0.2601
Original surface bottom	1	0.5796	0.6901	0.8015	1.2709
	2	0.5421	0.6521	0.7623	1.2461
	3	0.5013	0.6403	0.7415	1.2397
	4	0.5562	0.6709	0.7853	1.2603
	5	0.5487	0.6623	0.7779	1.2541
	6	0.5475	0.6507	0.7617	1.2405
	7	0.5694	0.6767	0.7902	1.2647
	8	0.5501	0.6715	0.7811	1.2579
	9	0.5723	0.6878	0.7963	1.2683
	max	0.5796	0.6901	0.8015	1.2709

Table 5: The surface defection.

The wheel Load (kN)	86.64	103.07	129.16	196.52
The surface defection (mm)	0.0816	0.0975	0.1069	0.1407

the entity, it is necessary to make the following basic assumptions [12]:

(1) The materials of each layer of the pavement structure are uniform, continuous, and isotropic linear elastic bodies characterized by the elastic modulus and Poisson's ratio

(2) The contact surface between the pavement slab and the basement and the basement and the soil foundation is assumed to be completely continuous with continuous contact between layers under the action of the wheel load

(3) The elastic modulus, Poisson's ratio, and other parameters of each layers' material do not change in the study

(4) Excluding the influence of the weight of each structural layer

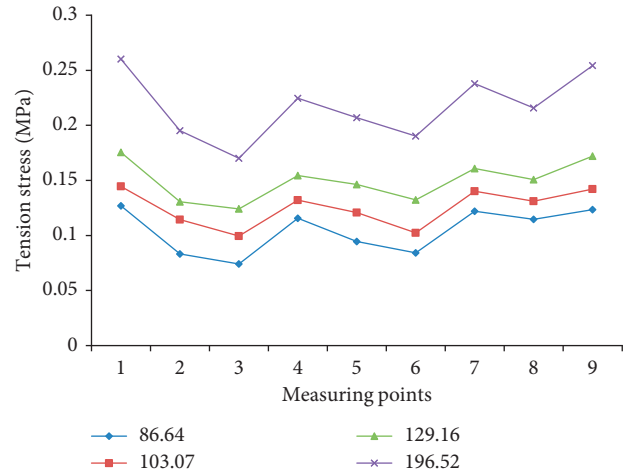

Figure 6: Tension stress value of each measuring point of the covered layer.

3.2. Preprocessing, Modeling, and Solving of FEM by ANSYS Software

3.2.1. Preprocessing of Contact Surface between Aircraft Wheel and Airport Pavement. The contact surface between the wheel and the airport pavement is actually an approximate ellipse with a rectangle in the middle and a semicircle on both sides. In the design of airport pavement, the contact surface is equivalent to a circle of equal area [1], as shown in Figure 10(a). However, this conversion method is difficult to be realized in the ANSYS software because it is not convenient for the meshing, and the coupling between the wheel and the pavement is bad, resulting in the inaccuracy of calculation results. In order to facilitate the finite element calculation and further improve the accuracy of the calculation, the approximate ellipse is converted into a square of equal area, as shown in Figure 10(b), and the square size after the conversion is shown in Table 6.

3.2.2. Unit and Material Definition. The model use SOILD65 unit commonly used in reinforced concrete engineering. The interaction between different layers is simulated by the contact unit. The rigid body target surface on the contact surface is TARGE170, and the contact surface is CONTA173 unit.

Define the thickness, elasticity modulus, Poisson's ratio, and density of different materials such as the new concrete

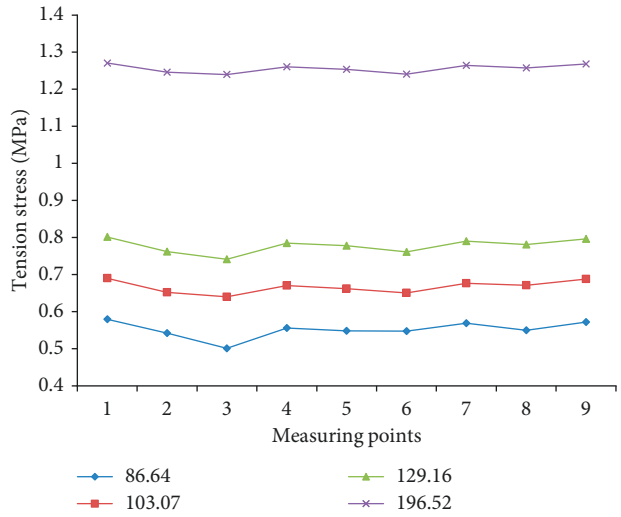

Figure 7: Tension stress value of each measuring point of the original surface layer.

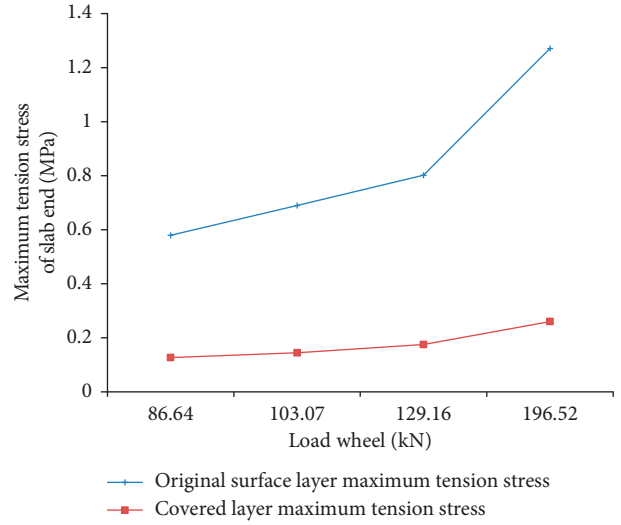

Figure 8: Maximum tension stress value of each measuring point.

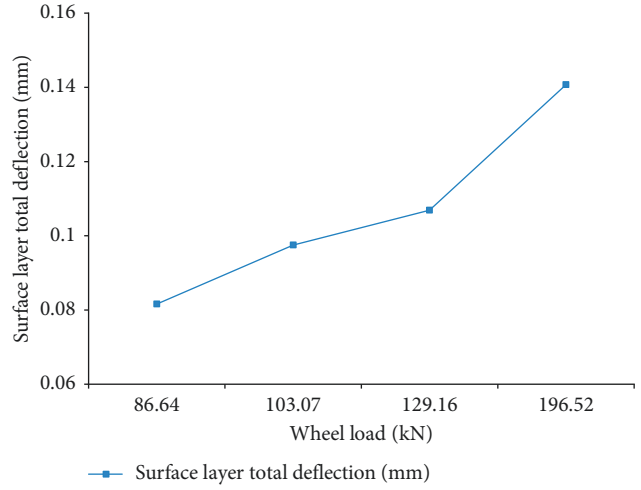

Figure 9: Maximum total defection values of each measuring point.

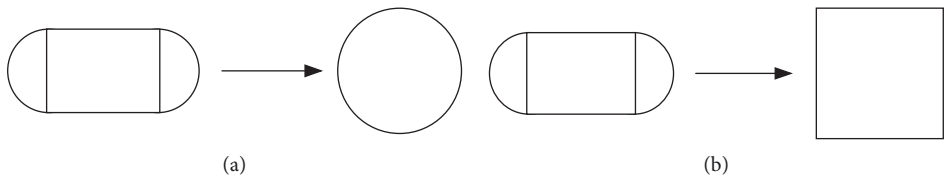

Figure 10: Conversion schematic diagram of the contact surface.

Table 6: Square size for various types od aircraft wheel.

Aircrafts	Single main wheel grounding area (cm^2)	Square size (cm)
A	1110.77	33.33
B	1171.25	34.22
C	2483.85	49.84
D	1284.44	35.84

pavement surface (the covered layer), the old concrete pavement surface (the original surface layer), the basement, and the soil foundation, as shown in Table 7.

3.2.3. Modeling. A 5 m × 5 m geometric model of a cement concrete slab is established, the length and width of which are half of the basement and the soil foundation and use the "SMART MESH" command to divide the grid to form a FEM, as shown in Figure 11.

3.2.4. Loading and Solving. Enter the solution module, impose constraints on the model, and set the analysis options. The displacement boundary is simulated with the actual consolidation of the pier bottom, and the temperature boundary is set at normal temperature (20°C). Gravity is loaded using the "ACEL" command, and concentrated force is loaded using the "F" command. A transient analysis is used to solve the dynamic effect.

3.3. FEM Results. Figures 12–15 show tension stress and maximum deflection with wheel load (each graph is composed of a two-dimensional broken line graph and a three-dimensional broken line graph).

Appendix A shows that stress analysis cloud chart under different wheel loads. As shown in Figures A1–A16, the deflection cloud diagram and the stress cloud diagram show roughly the same distribution rules that the middle of the slab longitudinal edge is the center, and the larger the radius is the smaller the deflection and stress values are, and the Y-direction maximum stress (i.e., the maximum tension stress) appears in the same position—the middle of the slab longitudinal edge, indicating that the critical position of ACCDDPS is in the middle of the longitudinal edge. We have listed Figures A1 and A3 as Figure 12(a) and Figure 12(b), respectively, and other pictures are shown in Appendix.

As depicted in Figures 13 and 14, the tension stress of covered layer increases with the increase of wheel load. When the load increases from 129.16 kN to 196.52 kN, the maximum tension stress increases to 0.257 MPa. That is, at

Table 7: The pavement material parameters.

Structural layer	Thickness (m)	Elastic Modulus (MPa)	Poisson ratio	Density (kg/m^3)
Covered layer	0.20	36000	0.15	2400
Original surface layer	0.30	32000	0.15	2400
Basement	0.40	300	0.25	2100
Soil foundation	10	80	0.35	1800

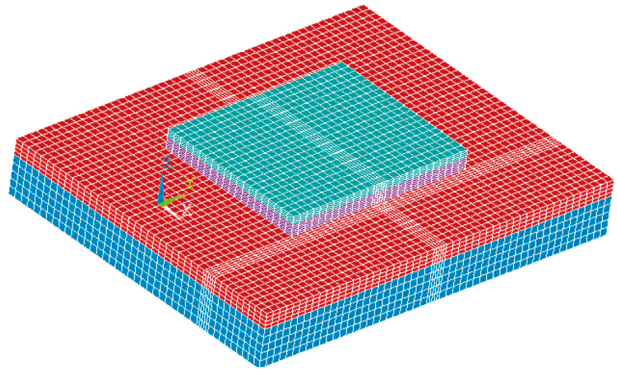

Figure 11: ACCDDPS FEM.

the point of 129.16 kN, there is a clear inflection point; after that point, the change rate of stress with load becomes larger. Similarly, the tension stress of original surface layer also increases with the increase of wheel load; however, at the point of 129.16 kN, the stress values of the three curves decrease slightly. Because the C-aircraft wheel load is 129.16 kN, the ground area of the wheel reaches 2483.85 cm^2 (it is nearly twice as high as the other three aircrafts) which decreases the stress. As we can see from Figures 13 and 14, for both covered layer and original surface layer, the principal stress curves almost coincide with the Y-direction stress curves, which means that the maximum principal stress of ACCSSPS is in the longitudinal direction.

Figure 15 shows that the maximum deflection values of the covered layer and the original surface layer increase with the increase of the wheel load. And, two maximum deflection curves almost coincide. This is in line with the mechanical principle of the combination method of the ACCDDPS.

3.4. FEM Verification. By comparing FEM and ARSTS experimental results, their experimental results are basically consistent, indicating that FEM is feasible for mechanical analysis of ACCDDPS. The following conclusions can be drawn:

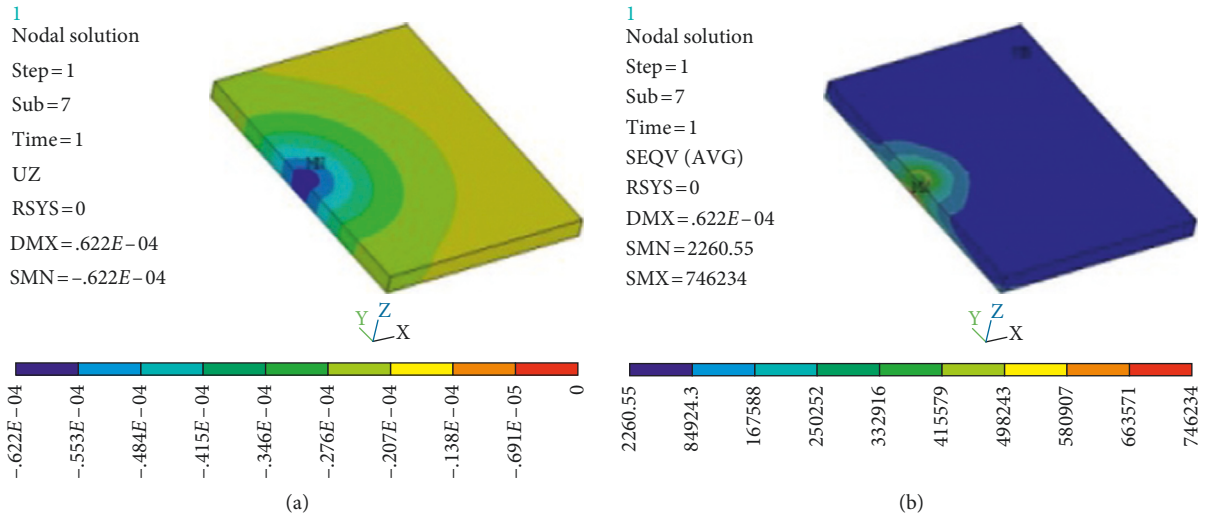

Figure 12: Aircraft deflection and stress cloud diagrams: (a) original surface layer deflection cloud diagram; (b) original surface layer stress cloud diagram.

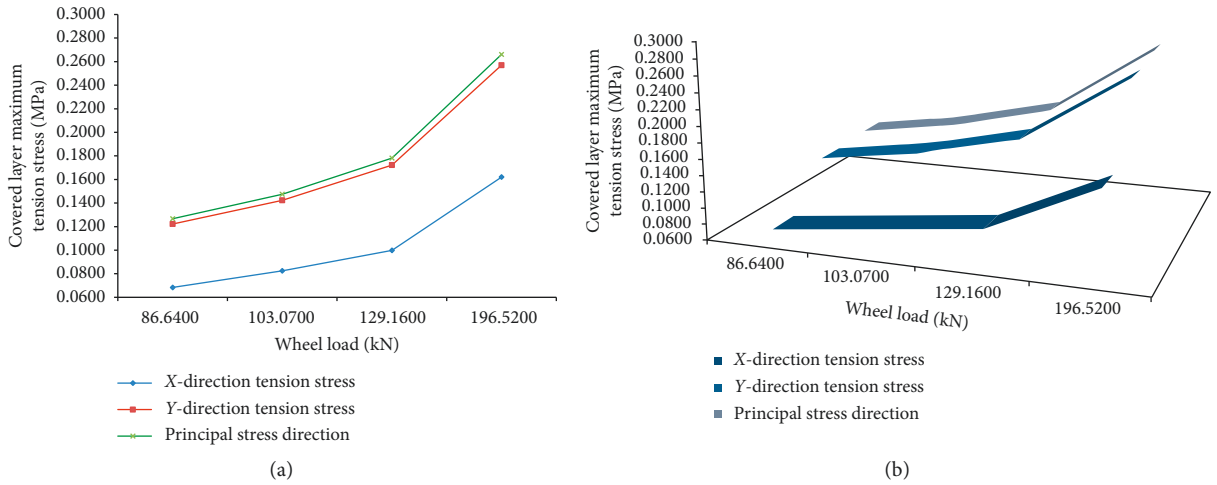

Figure 13: Variation of covered layer tension stress with the wheel load: (a) two-dimensional broken-line graph; (b) three-dimensional broken-line graph.

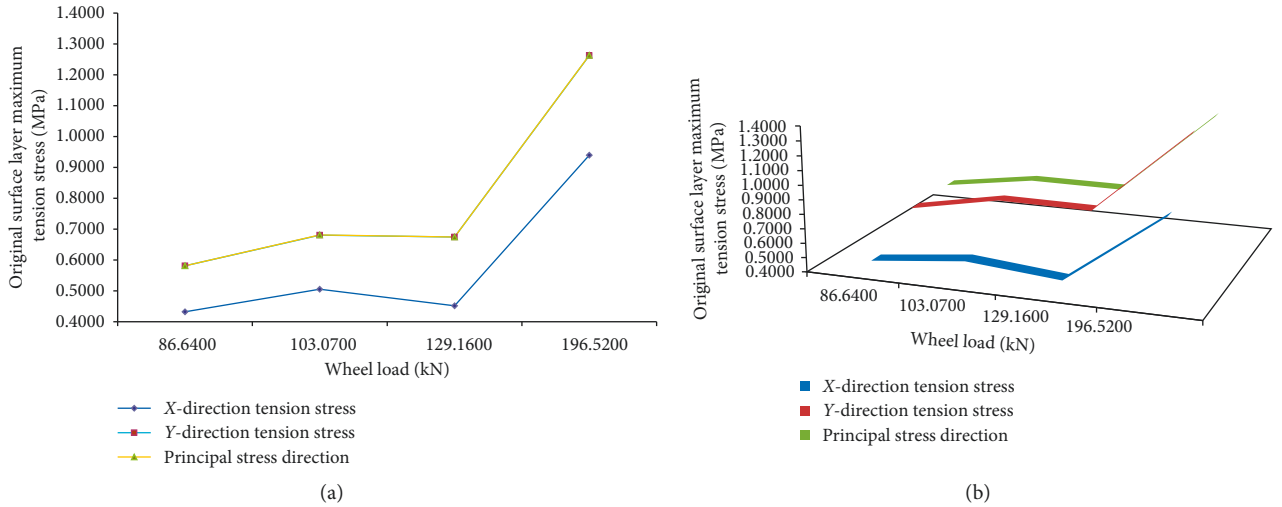

Figure 14: Variation of original surface layer tension stress with wheel load: (a) two-dimensional broken-line graph; (b) three-dimensional broken-line graph.

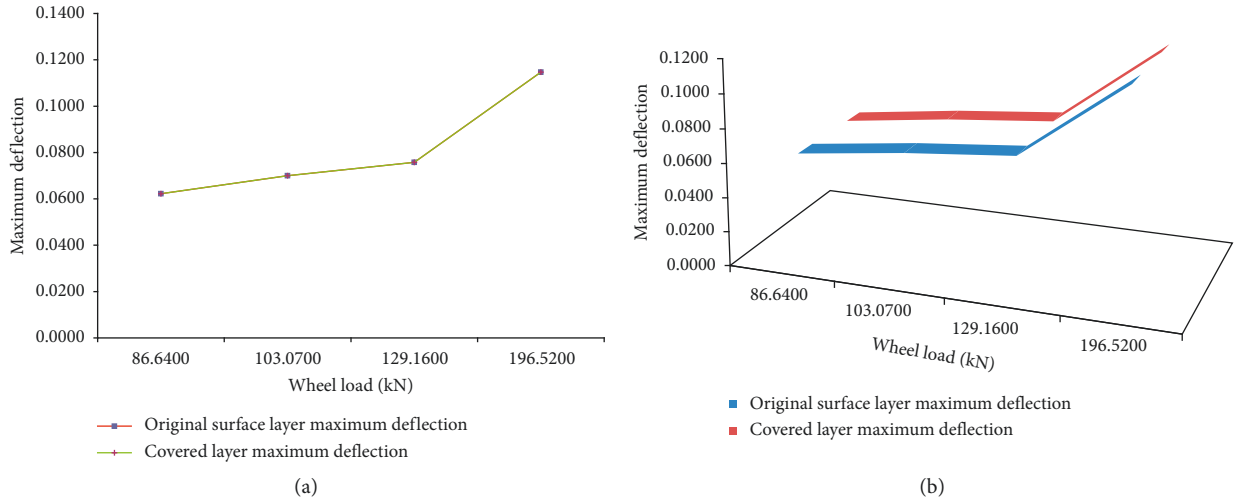

Figure 15: Variation of maximum deflection with wheel load: (a) two-dimensional broken-line graph; (b) three-dimensional broken-line graph.

(1) In the ANSYS stress cloud diagrams, the Y-direction maximum stress (i.e., the maximum tension stress) appears at the middle of the slab longitudinal edge. This is consistent with the results of the ARSTS experimental results—the maximum tension stress appears at the measuring point 1, namely, the middle of the slab longitudinal edge.

(2) Both FEM and ARSTS experiment results' maximum tension stress increases with the increase of wheel load, maximum deflection values of the covered layer and the original surface layer increases with the increase of the wheel load, and the point of 129.16 kN is a key point in the growth rate, which shows that ARSTS experimental results and FEM results are in good agreement.

The conclusions we obtained have a good fit with the existing results. Many experts and scholars agree that the critical load location of airport pavement and highway surface should coincide with the middle of the longitudinal joint, which coincides with our conclusion [1, 13]. Wong [14] used the theoretical formula to derive and came to such a conclusion that the maximum stress value of ACCDDPS is 0–2.35MPa. Our ARSTS experimental results and FEM results are within its range, which proves our research results have certain credibility.

4. Influences of Pavement Structure Parameters on Mechanical Properties of ACCDDPS

The above research shows that FEM is feasible and accurate for mechanical analysis of ACCDDPS. With the help of ANSYS software, we use the same FEM modeling method to further study the effect of three pavement structure parameters: covered layer thickness, elastic modulus, and slab size on mechanical properties of ACCDDPS, thus enriching and perfecting the design theory of ACCDDPS.

4.1. Covered Layer Thickness on Mechanical Properties of ACCDDPS. The covered layer thickness is 0.13 m, 0.15 m, 0.17 m, 0.19 m, 0.21 m, 0.23 m, 0.25 m, 0.27 m, 0.29 m, and 0.31 m, the slab size is 5 m × 4 m, and the load is 196.52 kN. The action area is 1284.44 cm^2. The other material parameters are shown in Table 7. The modeling method is as described above.

Figures 16–18 show tension stress and maximum deflection with covered layer thickness (each graph is composed of a two-dimensional broken-line graph and a three-dimensional broken-line graph).

Appendix B shows that stress analysis cloud chart under different covered layer thickness. As shown in Figures B1–B40, the deflection cloud diagram and the stress cloud diagram also show that the critical position of ACCDDPS is in the middle of the longitudinal edge.

As depicted in Figures 16 and 17, for both covered layer and original surface layer, the tension stress decreases with the increase of covered layer thickness. However, with the thickness of cover layer decreasing, the rate of stress reduction is different. For the covered layer, the decrease of principal stress is small, but for the original surface layer, the principal stress decreases faster. The principal stress curves almost coincide with the Y-direction stress curves, which means that the maximum principal stress of ACCDDPS is in the longitudinal direction.

Figure 18 shows the maximum deflection values of the covered layer, and the original surface layer decreases with the increase of covered layer thickness, and the deflection value is about 0.1 mm. From 13 cm to 31 cm, the maximum deflection value decreased by 24%. And two maximum deflection curves almost coincide. This is in line with the mechanical principle of the combination method of the ACCDDPS.

4.2. Covered Layer Elastic Modulus on Mechanical Properties of ACCDDPS. The covered layer elastic modulus is 24000 MPa, 26000 MPa, 28000 MPa, 30000 MPa,

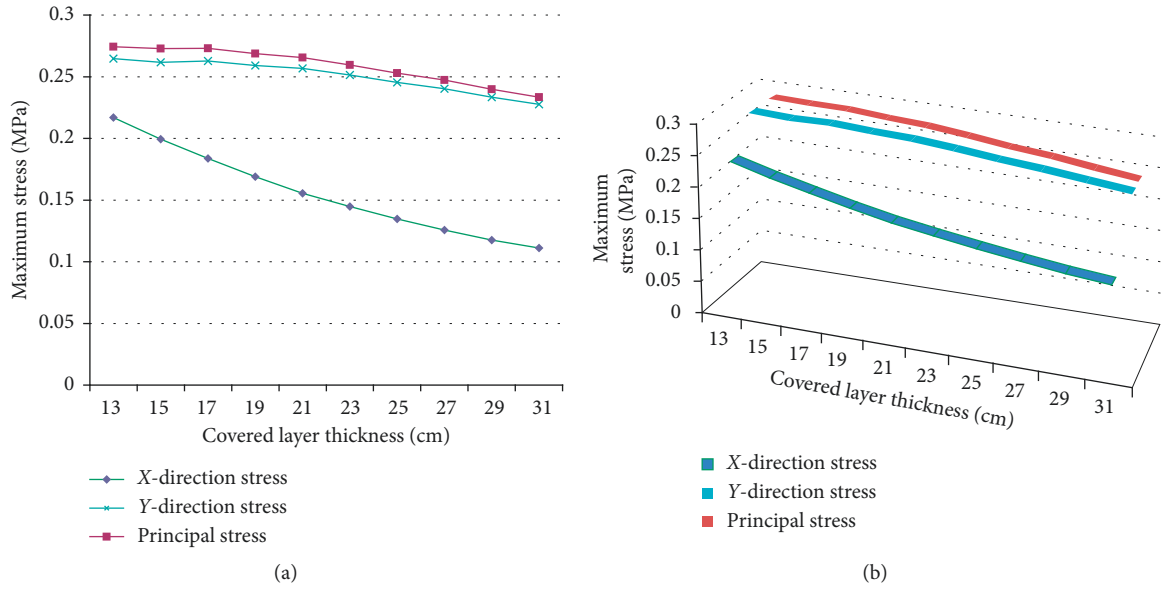

Figure 16: Variation of covered layer stress with covered layer thickness: (a) two-dimensional broken-line graph; (b) three-dimensional broken-line graph.

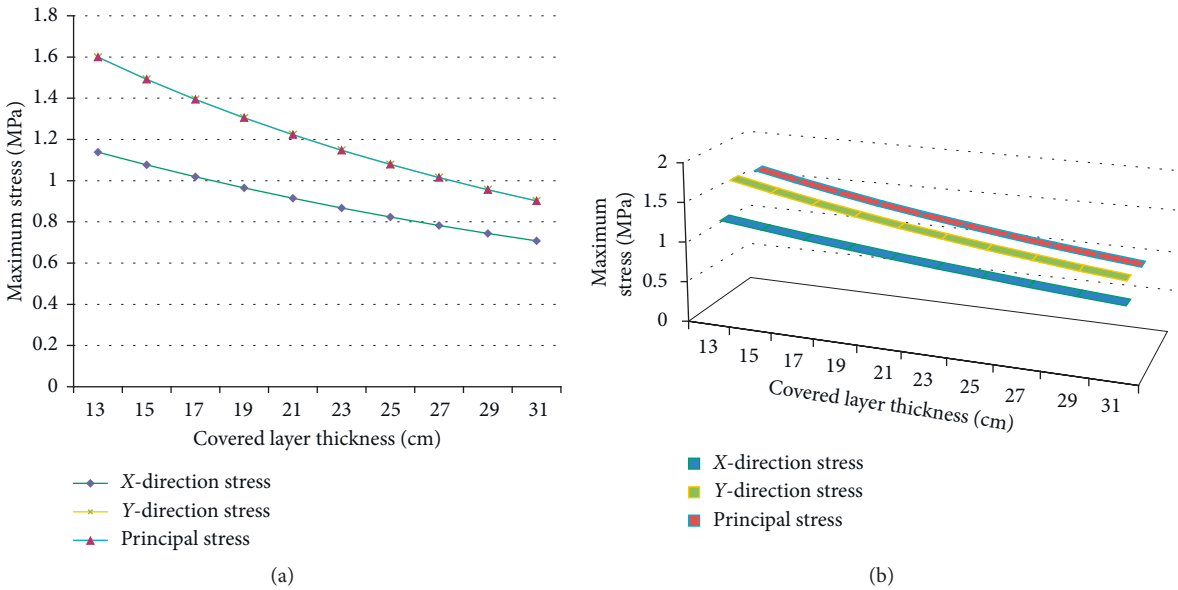

Figure 17: Variation of original surface layer stress with covered layer thickness: (a) two-dimensional broken-line graph; (b) three-dimensional broken-line graph.

32000 MPa, 34000 MPa, 36000 MPa, 38000 MPa, 40000 MPa, 42000 MPa, and 44000 MPa, the slab size is 5 m × 4 m, and the load is 196.52 kN. The action area is 1284.44 cm^2. The other material parameters are shown in Table 7. The modeling method is as described above.

Figures 19–21 show tension stress and maximum deflection with covered layer elastic modulus (each graph is composed of a two-dimensional broken-line graph and a three-dimensional broken-line graph).

Appendix C shows that stress analysis cloud chart under different covered layer thicknesses. As shown in Figures C1–C44, the deflection cloud diagram and the stress cloud diagram also show that the critical position of ACCDDPS is in the middle of the longitudinal edge.

As depicted in Figures 19 and 20, the principal stress curves almost coincide with the Y-direction stress curves, which means that the maximum principal stress of ACCDDPS is in the longitudinal direction. For covered layer, the tension stress increases with the increase of covered layer elastic modulus. However, for original surface layer, the tension stress decreases with the increase of covered layer elastic modulus.

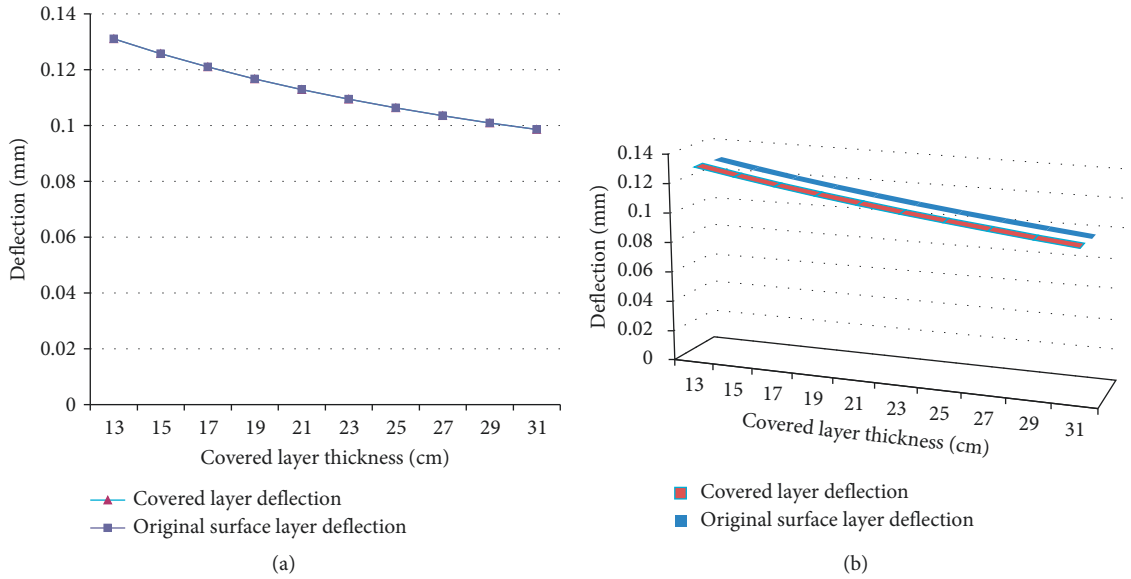

Figure 18: Variation of maximum deflection with covered layer thickness:. (a) two-dimensional broken line graph; (b) three-dimensional broken-line graph.

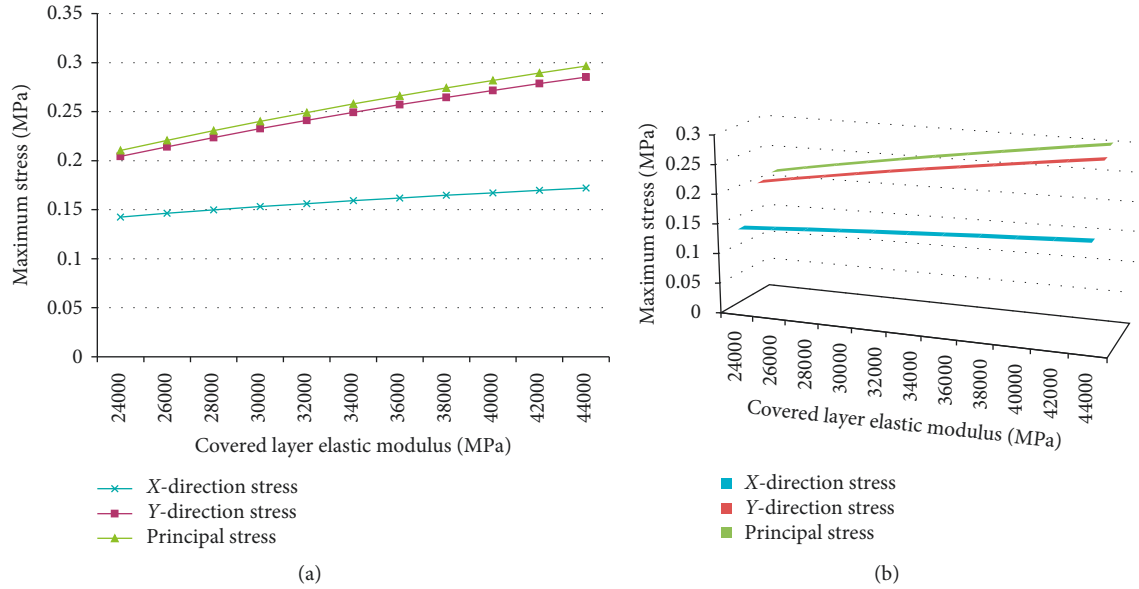

Figure 19: Variation of covered layer stress with covered layer elastic modulus: (a) two-dimensional broken-line graph; (b) three-dimensional broken-line graph.

Figure 21 shows that the maximum deflection values of the covered layer and the original surface layer decrease with the increase of covered layer elastic modulus, and the deflection value is about 0.1 mm. And, two maximum deflection curves almost coincide, which is determined by the mechanical principle of the combination method of the ACCDDPS.

4.3. Slab Size on Mechanical Properties of ACCDDPS. We select four common slab sizes (6 m × 5 m, 5 m × 5 m, 5 m × 4 m, 4 m × 4 m, resp.), and the load is 196.52 kN. The action area is 1284.44 cm^2. The other material parameters are shown in Table 7. The modeling method is as described above.

Figures 22–24 show tension stress and maximum deflection with slab size (each graph is composed of a two-dimensional broken-line graph and a three-dimensional broken-line graph).

Appendix D shows stress analysis cloud chart under different slab sizes. As shown in Figures D1–D16, the deflection cloud diagram and the stress cloud diagram also show that the critical position of ACCDDPS is in the middle of the longitudinal edge.

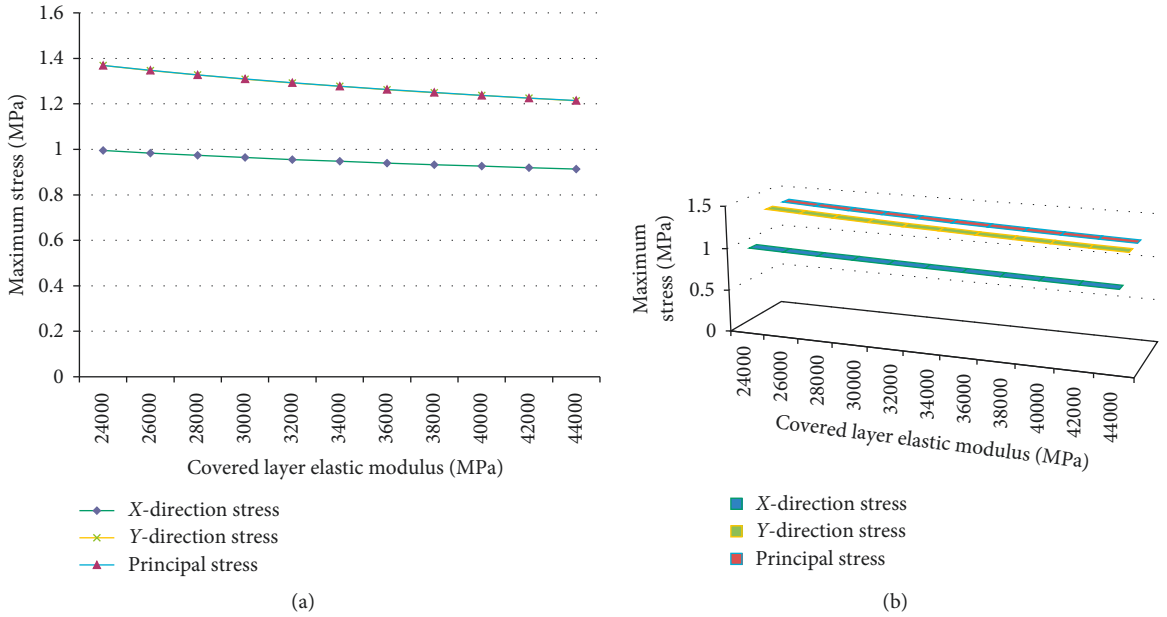

Figure 20: Variation of original surface layer stress with covered layer elastic modulus.

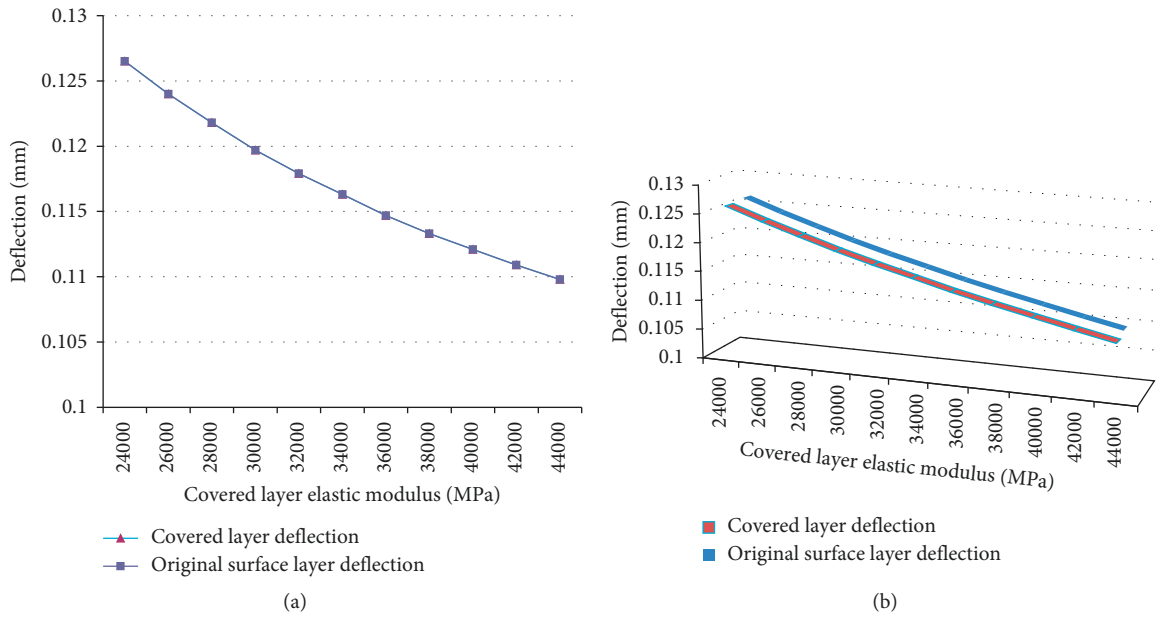

Figure 21: Variation of maximum deflection with covered layer elastic modulus.

As depicted in Figures 22 and 23, the principal stress curves almost coincide with the Y-direction stress curves, which means that the maximum principal stress of ACCDDPS is in the longitudinal direction. For covered layer, the tension stress decreases with the increase of slab size. However, for original surface layer, the tension stress hardly changes as the slab size increases.

Figure 24 shows the maximum deflection values of the covered layer, and the original surface layer increases with the increase of slab size, and the deflection value is about 0.1 mm. And, two maximum deflection curves almost coincide, which is determined by the mechanical principle of the combination method of the ACCDDPS.

5. Conclusions

We used the ARSTS to study the mechanical properties of ACCDDPS under aircraft single-wheel dynamic loads. In the ANSYS software, FEM was established and the simulation experiment under the same conditions was carried out. FEM results are consistent with ARSTS results and are consistent with the existing research conclusions, which prove the

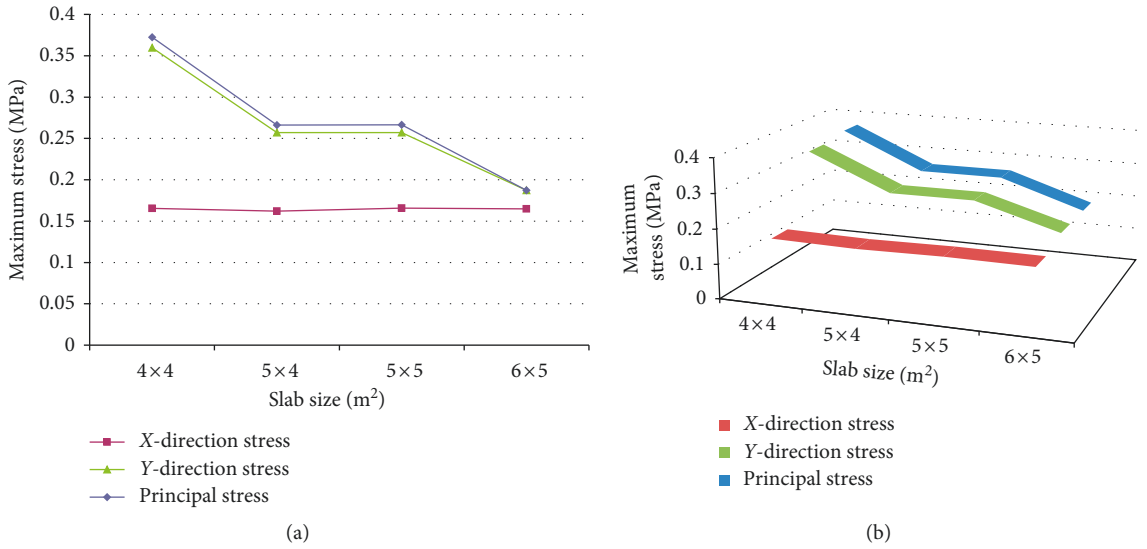

Figure 22: Variation of covered layer stress with slab size: (a) two-dimensional broken-line graph; (b) three-dimensional broken-line graph.

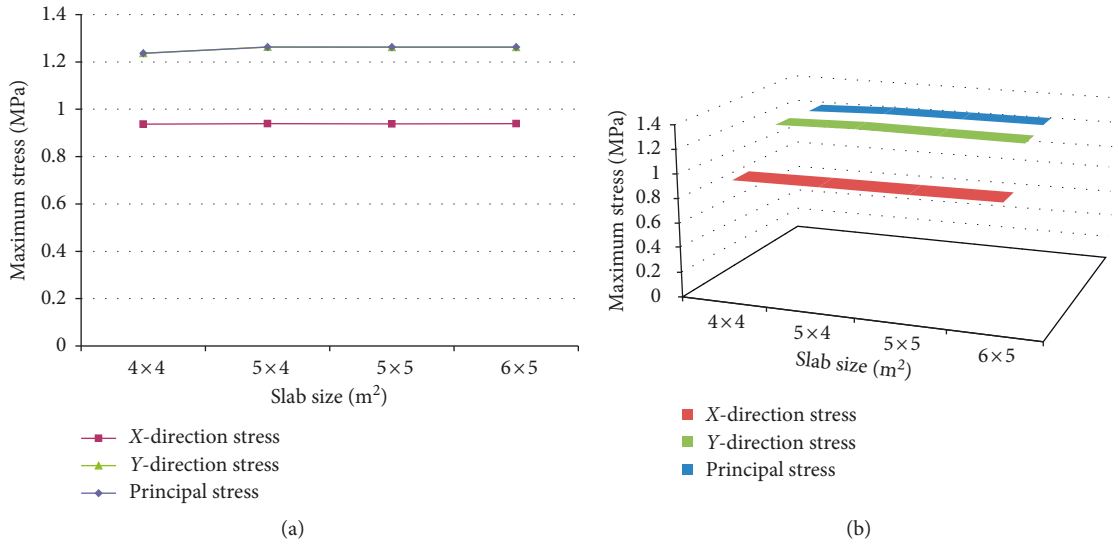

Figure 23: Variation of original surface layer stress with slab size: (a) two-dimensional broken-line graph; (b) three-dimensional broken-line graph.

feasibility of FEM applying ACCDDPS mechanical properties analysis. In view of this, we used FEM to analyze the influence of covered layer thickness, covered layer elastic modulus, and slab size on ACCDDPS mechanical properties. We find the following conclusions:

(1) Under the different loads, the change of the tension stress and deflection values with the load change is the same for the covered layer and the original surface layer. The critical position of ACCDDPS is in the middle of the longitudinal edge. The total deflection of surface layer increases with the increase of wheel load, and two maximum deflection curves almost coincide, which is in line with the mechanical principle of the combination method of the ACCDDPS.

(2) Although the structural parameters are different, the critical position of ACCDDPS is in the middle of the longitudinal edge, which may be determined by the slab geometry or load position. However, for the covered layer and the original surface layer, the law that the tension stress values vary with the structural parameters is different, but the maximum deflection value is about 0.1.

(a) The tension stress decreases with the increase of covered layer thickness, and the maximum deflection values decrease with the increase of covered layer thickness.

(b) For covered layer, the tension stress increases with the increase of covered layer elastic modulus. However, for original surface layer, the tension

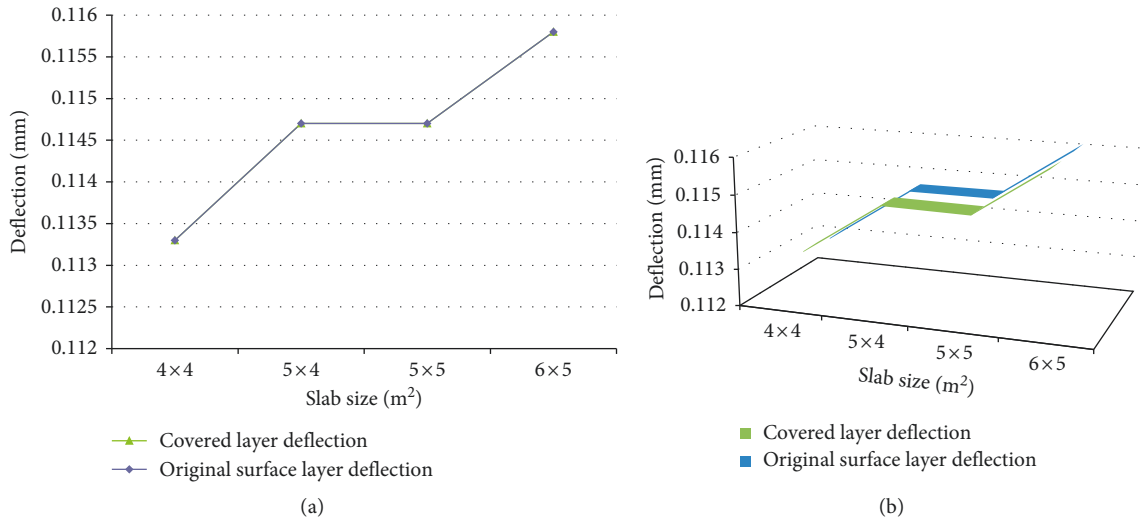

Figure 24: Variation of maximum deflection with slab size.

stress decreases with the increase of covered layer elastic modulus. The maximum deflection values decrease with the increase of covered layer elastic modulus.

(3) For covered layer, the tension stress decreases with the increase of slab size. However, for original surface layer, the tension stress hardly changes as the slab size increases. The maximum deflection values increase with the increase of slab size.

Data Availability

The data used to support the findings of this study are available from the corresponding author upon request.

Conflicts of Interest

The authors declare that they have no conflicts of interest.

Authors' Contributions

Yu Qingkun designed models and wrote the manuscript. Liangcai Cai analyzed the results. Jianwu Wang conducted data collection and statistics.

Supplementary Materials

The "Appendix" file contains the cloud diagrams we got from the finite element simulation of ANSYS software, because there are 116 pictures in total, so it is placed in the appendix for the reviewers to refer to. The main contents of the Appendix are as follows: Appendix A shows stress analysis cloud chart under different wheel loads, including Figures A1–A16. Appendix B shows stress analysis cloud chart under different covered layer thicknesses, including Figures B1–B40. Appendix C shows stress analysis cloud chart under different covered layer thickness, including Figures C1–C44. Appendix D shows stress analysis cloud chart under different slab sizes, including Figures D1–D16. (*Supplementary Materials*)

References

[1] W. Xingzhong and C. Liangcai, *Airport Pavement Surface Design*, China Communication Press, Beijing, China, 2007.

[2] V. A. Patil, V. A. Sawant, and K. Deb, "2-D finite element analysis of rigid pavement reason dynamic vehicle–pavement interaction effects," *Applied Mathematical Modeling*, vol. 37, no. 3, pp. 1282–1294, 2013.

[3] J. Binchen, Y. Jie, and Y. Ge, "Study on the method of establishing the finite element model of cement concrete pavement of airport," *Science and Technology Research*, vol. 5, no. 5, pp. 208–210, 2013.

[4] W. Shuyu, "Analysis of load stress of double-deck concrete pavement on elastic half space foundation," *Heilongjiang Traffic Science and Technology*, vol. 28, no. 2, p. 65, 2013.

[5] H. Chao, S. Jian, Y. Jianming et al., "Research on the influence of old pavement fragmentation and addition mode on cement overlay," *Chinese and Foreign Highway*, vol. 34, no. 2, pp. 109–112, 2014.

[6] Z. Haiyan, W. Xuancang, Y. Dianhai et al., "Force analysis of finite size composite pavement slab on elastic foundation," *Journal of Shenyang University of Architecture (Natural Science)*, vol. 24, no. 1, pp. 6–10, 2008.

[7] Y. Xiangcheng, W. Xingzhong, Z. Ying et al., "Force analysis on the Fiber Grill Reinforced Airport Double-deck Pavement," *Journal of Wuhan University of Technology (Transportation Science and Engineering Edition)*, vol. 36, no. 5, pp. 954–957, 2012.

[8] Z. Xianmin, D. Qian, and L. Yaozhi, "The influence of the aircraft landing-gear configuration on the mechanical response of the pavement surface," *Journal of Southwest Jiaotong University*, vol. 49, no. 4, pp. 675–681, 2014.

[9] L. Zizheng and Z. Hongduo, "Structural response analysis of composite pavement under A380-800 aircraft load," *Western Communication Technology*, vol. 79, no. 2, pp. 69–74, 2014.

[10] M. Xiang, N. Fujian, and C. Rongsheng, "Composite airport pavement surface load stress," *Journal of Chang'an University (Natural Science Edition)*, vol. 30, no. 4, pp. 23–28, 2010.

[11] S. Choi, J. Yeon, and M. C. Won, "Improvements of curing operations for Portland cement concrete pavement," *Construction and Building Materials*, vol. 35, no. 10, pp. 597–604, 2012.

[12] A. Zokaei-Ashtiani, C. Carrasco, and S. Nazarian, "Finite element modeling of slab–foundation interaction on rigid pavement applications," *Computers and Geotechnics*, vol. 62, pp. 118–127, 2014.

[13] S. Jiankang, W. X. Zhong, and Y. Xiangcheng, "Test method for airport cement concrete double deck pavement sandwich material," *Sichuan Building Science*, vol. 38, no. 1, pp. 171–174, 2012.

[14] MH/T5004-2010, *Specifications for Airport Cement Concrete Pavement Design*, Civil Aviation Administration of China, Beijing, China, 2010.